Contrib. Plasma Phys. **54**, No. 4-6, 454 – 458 (2014) / **DOI** 10.1002/ctpp.201410055

Multi-Fluid Transport Modeling of NSTX Upgrade Standard and Snowflake Divertor Configurations

E. T. Meier[1]*, **V. A. Soukhanovskii**[1], **S. Gerhardt**[2], **J. E. Menard**[2], and **T. D. Rognlien**[1]

[1] Lawrence Livermore National Laboratory, Livermore, California 94551, USA
[2] Princeton Plasma Physics Laboratory, Princeton, New Jersey 08540, USA

Received 15 October 2013, revised 14 November 2013, accepted 14 November 2013
Published online 12 June 2014

Key words NSTX-U, divertor, UEDGE, snowflake, impurity seeding, cryopump.

In NSTX Upgrade (NSTX-U), power exhaust is expected to challenge available material and heat removal technologies, which are limited to $\sim$10 MW/m^2. Preliminary analysis of heat flux mitigation strategies, including the snowflake divertor configuration and radiative divertor operation, is performed with the multi-fluid edge transport code, UEDGE. Divertor recycling between 95% and 99%, and power exhaust between 7 and 9 MW are explored. Compared to the standard divertor, the particular snowflake divertor studied here strongly reduces outer target heat flux, but tends to have higher ($>$10 MW/m^2) inner target heat flux. This suggests that snowflake divertor optimization should be pursued in future work. Both neon and argon impurity seeding scenarios mitigate high heat fluxes in both standard and snowflake configurations, but argon can cause radiative collapse of the core plasma at only 3% concentration. Divertor cryopumping is also considered, and modeling shows $\sim$50% more particle removal with the snowflake divertor.

1 Introduction

Heat flux management is critical for ITER and other next-step tokamaks. Power exhaust to the scrape-off layer (SOL) will rise dramatically [1], while the width of the SOL that transmits power to divertor targets is expected to contract [2]. In the National Spherical Tokamak Experiment (NSTX), heat flux width measured in the outer midplane (λ_q) was found to scale inversely with the plasma current: $\lambda_q \propto I_p^{-1.6}$ [3]. NSTX Upgrade (NSTX-U) [4], scheduled to begin operation in 2014, will have twice the plasma current of NSTX (2 MA vs. 1 MA), and more than twice the neutral beam power ($\lesssim$ 15 MW vs. 6 MW). Thus, the unmitigated peak heat flux in NSTX-U is projected to be several times higher than in NSTX, easily exceeding the approximate 10 MW/m^2 limit dictated by solid material and heat removal technologies. Such heat loading represents both an opportunity—to contribute to the physics basis for ITER and beyond—and a major challenge.

This paper describes preliminary analysis of mitigation strategies, focusing on the snowflake divertor (SFD) [5, 6] and impurity seeding, which has been conducted using the multi-fluid edge transport code, UEDGE [7, 8], with the goal of addressing a variety of divertor scenarios expected in NSTX-U. A progression of plasma-facing components, from purely graphite to purely high-Z (e.g., molybdenum), is planned. Divertor target surfaces may be bare, or conditioned with lithium or boron. Also, a divertor cryopump is planned as a means to control density buildup [4].

2 Snowflake overview

The snowflake divertor (SFD) [5,6] involves introducing a secondary X-point near the primary X-point (resulting in a separatrix structure with a six-fold "snowflake" appearance). Exact snowflakes, in which the primary and secondary X-points coincide, are possible with sufficient control, but the secondary X-point is generally located on either the private flux side, or the scrape-off layer side of the separatrix, forming snowflake plus (SFD$^+$), and snowflake minus (SFD$^-$) configurations, respectively. Three ways in which heat flux reduction in the SFD may

* Corresponding author. E-mail: meier23@llnl.gov, Phone: (609) 243-2950, Fax: n/a

occur are: (1) Increased plasma-wetted area (A_{wet}) resulting from flux expansion. Heat flux is reduced in direct proportion to A_{wet}. (2) Elongation of the magnetic connection length (L_C). Two-point model analysis [9] shows that longer L_C promotes lower target temperature ($T_t \sim L_C^{-4/7}$), which often leads to increased radiation. (3) Increased divertor volume (V_{div}). Total divertor radiation scales directly with V_{div}. Modeling has shown the effectiveness of the SFD in mitigating heat flux through these three channels [10].

The SFD concept has been demonstrated on several tokamaks, including TCV [11], NSTX [12], and DIII-D [13]. On NSTX, partially-detached divertor plasmas with large heat flux reduction have been observed in SFD$^-$ configurations with the secondary X-point located near the outer strike point.

3 UEDGE modeling setup

UEDGE [7, 8] is a 2D multi-fluid edge transport code, based on the classical two-fluid ion-electron model of Braginskii [14]. Perpendicular transport is diffusive with parameterized transport coefficients. A fluid neutral model is used, with Navier-Stokes-like parallel neutral momentum and cross-field charge-exchange diffusion.

Grids are based on equilibria generated with ISOLVER, a Grad-Shafranov equilibrium code. The grid used for the NSTX-U SD simulations is shown in Figure 1. The SD and SFD grids span normalized flux $\psi_n = 0.9-1.055$. The grids are narrow at the outer midplane (OMP), where the scrape-off layer (SOL) thickness is 0.9 cm. As a result, solutions can be sensitive to the outer wall boundary conditions. (A thicker SOL is possible only if the upper magnetic null is accomodated in the modeling; such an extension is left for future work.) High-field side (i.e., inner wall) gas injection, Γ_G, is included as shown.

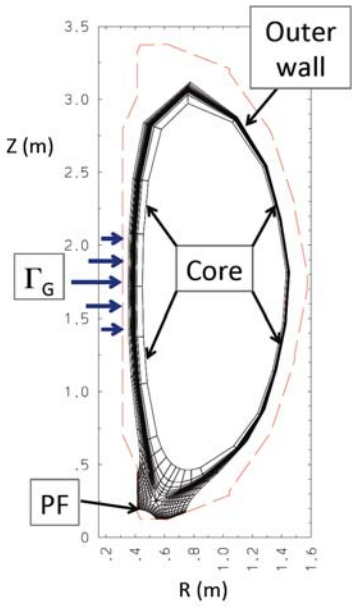

Fig. 1 Flux-aligned UEDGE grid for standard divertor (SD) simulation. The outer wall, private flux region (PF), and core boundaries are indicated. Distributed gas injection, Γ_G, is included as shown.

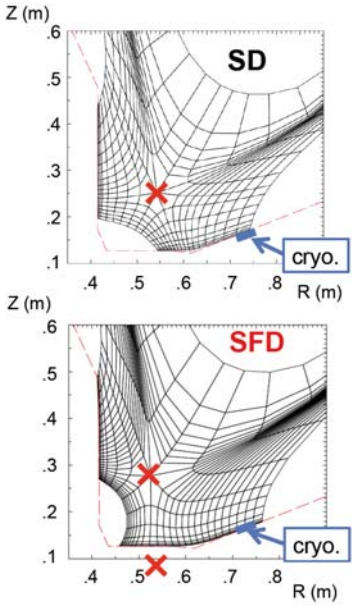

Fig. 2 Close-up view of SD and SFD grids. Divertor cryopumping is modeled at the locations indicated. The primary and secondary SFD X-points are identified with red X's.

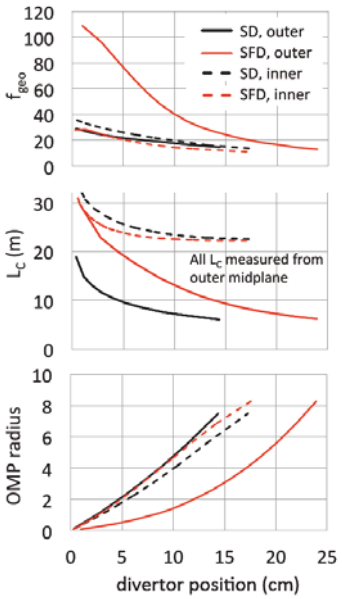

Fig. 3 Geometric broadening (f_{geo}), connection length (L_C), and outer midplane (OMP) radius (relative to the separatrix) for the SFD and SD plotted as a function of divertor target position (relative to the separatrix).

Divertor regions of SD and SFD grids are shown in Figure 2. Cryopump duct entrances are ∼3 cm wide, located at major radius $R = 0.72$ m. Neutral "albedo" is set to 0.5 at the duct entrances, i.e., 50% of neutral particles that impinge on the modeled cryopump duct are removed.

A criterion for a SFD is that $d_{sf}/\lambda_q^X \lesssim 1$, where d_{sf} is the distance between the primary and secondary X-points, and λ_q^X is the heat flux width mapped to the primary X-point [15]. For the SFD shown in Figure 2, $d_{sf}/\lambda_q^X = 1.2$. Characteristic SFD effects may not be as strong as for a more optimized SFD.

Flux expansion characteristics for the SD and SFD are presented in Figure 3. Poloidal flux expansion is defined as $f_{exp} \equiv (RB_{pol})_{OMP}/(RB_{pol})_{targ.}$, where the product of major radius (R) and poloidal magnetic field (B_{pol}) is evaluated at the outer midplane (OMP) and at the target. The total geometric increase in plasma wetted area is $f_{geo} = f_{exp}/\sin(\alpha)$, where α is the angle in the poloidal plane of field lines with respect to the target. The magnetic connection length, L_C, from the OMP to the divertor targets is also shown in Figure 3. The SD and SFD studied here are based on configurations presented in a recent overview of NSTX-U [4].

Power input through the core boundary is split evenly between ion and electron channels. Power input levels $P_{core} = 7$, 9, and 11 MW are studied. Particle input through the core boundary is 20 A/MW of input power (where "A" refers to the amp-equivalent current assuming each particle carries 1 C charge). Divertor target recycling coefficients between 95% and 100% are used to model scenarios with significant target pumping as expected with boron and lithium conditioning, and scenarios with saturated divertor targets. Fixed fraction carbon impurity is used except for the argon and neon impurity scans. The carbon concentration is 5% of deuterium density. Coronal radiation is assumed. Scans of argon and neon seeded impurity also assume coronal fixed fraction radiation. The seeded impurity scans, which have no carbon radiation, are representative of scenarios with high-Z walls.

Perpendicular particle diffusivity (D) is assumed to be similar to transport levels determined by analysis of NSTX discharges (e.g., [16]). Inside the separatrix, $D \propto (r - r_c)^3$ is assumed, where the r is the radial direction (i.e., the direction normal to flux surfaces), and r_c is the radius of the core boundary. At the core boundary, $D = 0.1$ m^2/s, and $D = 0.5$ m^2/s at the separatrix. In the SOL, $D = 0.5$ m^2/s. Perpendicular thermal diffusivity (χ) is chosen to give $\lambda_q = 3.0$ mm, as expected from the NSTX scaling [3]. Thermal diffusivity varies as $\chi \propto (r - r_c)^3$ from $\chi = 1$ m^2/s at the core, to a separatrix value of $\chi = 3$ m^2/s. In the SOL, $\chi = 3$ m^2/s. For SD simulations, this χ profile gives $2 < \lambda_q < 4$ mm across the range of power and divertor target recycling studied. Ion and electron perpendicular thermal diffusivities are assumed to be equal ($\chi_i = \chi_e = \chi$).

Other relevant boundary conditions and settings are as follows: T_e and T_i are fixed to 20 eV at the outer wall; 5-cm gradient length scale boundary conditions are used for density at the outer PF walls, and for T_e and T_i at the PF wall; 25% recycling is used at the outer and PF walls; neutral pumping is not used except at the cryopump ducts; plasma cross-field drift effects are not included.

4 Results and discussion

4.1 Operating space scans

Figure 4 shows the performance of SD and SFD configurations for divertor recycling $0.95 < R_{div} < 0.99$, and for $P_{core} = 7$, 9, and 11 MW. In these simulations, the high-field-side gas injection is $\Gamma_G = 400$ A. SFD outer target peak heat fluxes ($q_{pk,o}$) are generally less than q_{lim} ($q_{lim} \equiv 10$ MW/m^2). SD outer target peak heat flux ($q_{pk,o}$), generally exceeds q_{lim}. Inner target peak heat flux ($q_{pk,i}$) generally exceeds q_{lim} for both SD and SFD cases. At the highest recycling level, $R_{div} = 0.99$, inner divertor detachment occurs (i.e., target $T_e < 5$ eV).

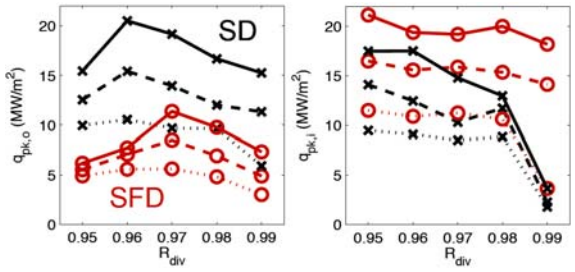

Fig. 4 Peak heat flux on the outer ($q_{pk,o}$, at left) and inner ($q_{pk,i}$, at right) divertor targets for SD and SFD scenarios for power input $P_{core} = 7$, 9, and 11 MW (dotted, dashed, and solid lines, resp.). $\Gamma_G = 400$ A for all runs.

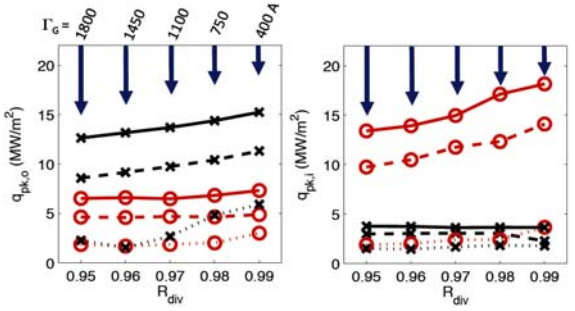

Fig. 5 Scan of recycling as shown in Figure 4, but with Γ_G increasing with reduced recycling.

To reduce $q_{pk,i}$, Γ_G is increased such that it varies from 400 A at $R_{div} = 0.99$ to 1800 A at $R_{div} = 0.95$. Results for a recycling scan with increased Γ_G are shown in Figure 5. For the SD at all input power levels, the

inner target remains detached with low $q_{pk,i}$. For the SFD, inner target detachment occurs for $P_{core} = 7$ MW, but not for the higher input powers. Note that the trend in q_{pk} (outer and inner) to higher values with increasing R_{div} is due to reduced Γ_G rather than higher R_{div}. (As seen in Figure 4, higher R_{div} leads to lower q_{pk} when Γ_G is fixed.)

Operation at low Greenwald fraction is critical to achieving the key NSTX-U goal of accessing low-collisionality regimes [4]. In the SD and SFD simulations presented in Figure 5, the deuterium contribution to the Greenwald fraction is reasonably low, ranging from $f^D_{GW} = 0.29$ (for $R_{div} = 0.95$) to $f^D_{GW} = 0.23$ (for $R_{div} = 0.99$). Here, $f^D_{GW} \equiv n_{ped}/n_{GW}$, where n_{ped} is taken to be three times the separatrix deuterium density.

The persistent attachment of the SFD inner divertor can be partly attributed to ∼20% less geometric expansion at the inner divertor target in the SFD case (see Figure 3). Also, the large SFD outer divertor flux expansion might affect the inner divertor. For a medium-power, medium-recycling case, Figure 6 shows SFD outer target plasma that is sheath-limited (i.e., divertor T_e within 10% of upstream T_e) over the first 10 cm, corresponding to the portion of the inner divertor target with $q_{pk,i} = 12$ MW/m^2. The corresponding SD outer target plasma exhibits high heat flux, but has temperatures < 50 eV, while the inner target plasma is detached. The physics leading to the sheath-limited SFD outer target are not clear, but modified neutral confinement could play a role.

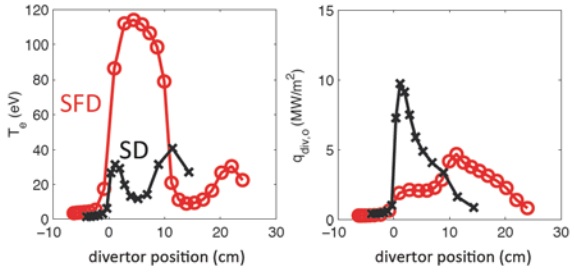

Fig. 6 Outer divertor target electron temperature and heat flux for SD and SFD cases with $P_{core} = 9$ MW, $R_{div} = 0.97$, and $\Gamma_G = 1100$ A.

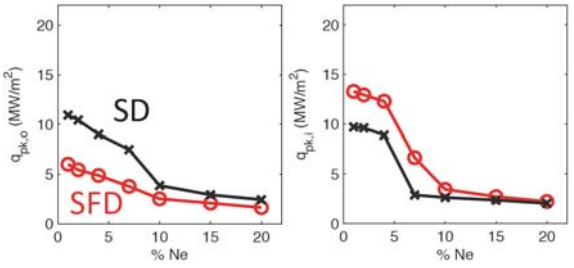

Fig. 7 Scan of neon impurity seeding at $P_{core} = 9$ MW and $R_{div} = 0.99$. A broad range of concentrations (6-20%) result in low $q_{pk,i}$ and $q_{pk,o}$.

4.2 Cryopumping

Simulations with divertor cryopumping are performed for $R_{div} = 0.95$-1.0 at $P_{core} = 9$ MW. For both SD and SFD cases, $q_{pk,o}$ and $q_{pk,i}$ are slightly higher than for corresponding runs without cryopumping. Particle removal is more effective in the SFD than in the SD. For example, at $R_{div} = 0.97$, the cryopumping rate, Γ_{cryo}, is 50% greater in the SFD case, with $\Gamma_{cryo} = 23\%$ and 15% of the total particle input in the SFD and SD, respectively. In flux space, the cryopump duct is slightly closer to the strike point in the SFD than in the SD; modified particle transport may also contribute to enhanced pumping. With $R_{div} = 1.0$, $q_{pk,i}$ in the SFD is dramatically reduced, and outer divertor target electron temperature is reduced to T_e <20 eV—comparable to T_e seen in the corresponding SD case.

Across the recycling space, f^D_{GW} in SD cryopumped simulations is ∼10-20% lower than in the corresponding cases without cryopumping. For the SFD, the reduction of f^D_{GW} is ∼15-25%.

4.3 Impurity seeding

Modeling of impurity seeding indicates that NSTX-U operation with low $q_{pk,i}$ and $q_{pk,o}$ is possible. With argon seeding, there is a narrow window around 2.5% Ar that yields the desired low q_{pk} values, but above 3% Ar, the core plasma radiatively collapses. With neon seeding, Figure 7 shows a broad operational low-q_{pk} window from 6-20% Ne. The reason for the relatively sudden radiative core collapse for argon seeding is that the radiation loss function ("cooling curve") for argon has a strong secondary peak at ∼200 eV [17]. The secondary peak for neon at ∼300 eV is an order of magnitude weaker.

5 Summary

For both SD and SFD scenarios, a broad NSTX-U operating space—with power exhaust from 7 to 11 MW and recycling between 95 and 100%—is explored with UEDGE using realistic power and particle input/output. Modeling indicates that operation with inner and outer divertor target heat fluxes less than 10 MW/m^2 is achievable if sufficient high-field-side gas injection (Γ_G) is employed. Even at the highest modeled Γ_G rates, the deuterium contribution to the Greenwald fraction (f_{GW}^D) is less than 0.3.

The particular SFD studied outperforms the SD in terms of outer divertor heat flux reduction, but inner divertor attachment (and heat fluxes $>$10 MW/m^2) is more problematic than in the SD. SFD optimization should be considered in future work. For example, The SFD could be tuned to have lower flux expansion, or the secondary X-point could be moved radially outward with respect to the strike point. Also of interest are SFD with secondary X-points within the plasma volume, located, e.g., within a few cm of the primary X-point instead of the $\sim$20-cm separation in the SFD studied here. Such close arrangement of SFD X-points would offer splitting of heat flux among four divertor legs instead of just two, and might enhance other SFD heat flux reduction effects. Also, modeling presented here does not address NSTX-U double-null operation, in which inner divertor targets will be protected from strong outboard heat exhaust, possibly maximizing the effectiveness of upper/lower SFD configurations. It is important to note that an expanded physics scope might be needed to fully understand SFD operation. For example, plasma cross-field drifts, and regions with low neutral collisionality could be important. Also, instabilities in regions with high poloidal plasma beta might locally enhance transport [18].

Cryopumping simulations show a strong effect on Greenwald fraction. For both SD and SFD, over the recycling range explored, f_{GW}^D is reduced by $\sim$20%. Simulations show 50% stronger cryopump particle removal for the SFD than for the SD.

Modeling reveals impurity seeding scenarios with successful heat flux mitigation. With argon seeding, a threshold in acceptable argon concentration ($\sim$3%) is found, beyond which the core plasma radiatively collapses. With neon, such a threshold is not seen up to 20% impurity concentration.

Acknowledgements We would like to thank D. Ryutov for snowflake theory insights. This work has been performed under the auspices of the U.S. Department of Energy by Lawrence Livermore National Laboratory under Contracts DE-AC52-07NA27344 and DE-AC02-09CH11466.

References

[1] J.E. Menard et al., Nucl. Fusion **51**,103014 (2011).
[2] T. Eich et al., Phys. Rev. Letters **107**, 215001 (2011).
[3] T.K. Gray et al., J. Nucl. Mater. **415**, S360 (2011).
[4] J.E. Menard et al., Nucl. Fusion **52**, 083015 (2012).
[5] D.D. Ryutov, Phys. Plasmas **14**, 064502 (2007).
[6] D.D. Ryutov, M.A. Makowski, and M.V. Umansky, Plasma Phys. Contr. Fusion **52**, 105001 (2010).
[7] T.D. Rognlien, J.L. Milovich, M.E. Rensink, and G.D. Porter, J. Nucl. Mater. **196**, 347 (1992).
[8] T.D. Rognlien and M.E. Rensink, Fusion Eng. Design **60**, 497 (2002).
[9] P.C. Stangeby, "The plasma boundary of magnetic fusion devices" IOP publishing Ltd., 2000.
[10] M. Umansky et al., Contrib. Plasma. Phys. **50**, 350 (2010).
[11] F. Piras et al., Plasma Phys. Control. Fusion **51**, 055009 (2009).
[12] V.A. Soukhanovskii et al., Nucl. Fusion **51**, 012001 (2011).
[13] D.N. Hill et al., Nucl. Fusion **53**, 104001 (2013).
[14] S.I. Braginskii, "Transport processes in a plasma", In M.A. Leontovitch, editor, Rev. Plasma Phys., Vol. 1, pages 205-311. Consultants Bureau, New York, NY, 1965.
[15] D.D. Ryutov, R.H. Cohen, T.D. Rognlien, and M.V. Umansky, Plasma Phys. Contr. Fusion **54**, 124050 (2012).
[16] J.M. Canik et al., J. Nucl. Mater. **415**, S409 (2011).
[17] H.P. Summers, "Atomic data and analysis structure" JET-IR(94)06, 1994.
[18] D.D. Ryutov R.H. Cohen, T.D. Rognlien, and M.V. Umansky, Contrib. Plasma Phys. **52**, 539 (2012).

